Journal of Alloys and Compounds 670 (2016) 1–11

Contents lists available at ScienceDirect

Journal of Alloys and Compounds

journal homepage: http://www.elsevier.com/locate/jalcom

Electronic structure and transport properties of $Ba_2Cd_2Pn_3$ (Pn = As and Sb): An efficient materials for energy conversion

A.H. Reshak [a, b, *]

[a] New Technologies - Research Centre, University of West Bohemia, Univerzitni 8, 306 14 Pilsen, Czech Republic
[b] Center of Excellence Geopolymer and Green Technology, School of Material Engineering, University Malaysia Perlis, 01007 Kangar, Perlis, Malaysia

ARTICLE INFO

Article history:
Received 6 September 2015
Received in revised form
30 January 2016
Accepted 1 February 2016
Available online 6 February 2016

Keywords:
Electronic properties
Transport properties
BoltzTraP code
mBJ
Energy conversion

ABSTRACT

The full potential method within the recently modified Becke-Johnson potential explore that the $Ba_2Cd_2Pn_3$ (Pn = As and Sb) compounds are narrow band gap semiconductors of about 0.49 and 0.32 eV, which confute the finding of the previous TB-LMTO-ASA calculation that $Ba_2Cd_2Sb_3$ is a poor metal. It has been found that there are subtle difference in band desperations of the two compounds, resulting in significant influence on the electronic and transport properties, taking into account the size and the electro-negativity differences between As and Sb atoms. Calculation show that there exists a strong hybridization between the orbitals which may lead to form covalent bonding which is more favorable for the transport of the carriers than ionic one. The electronic structure, the anisotropy and the inter-atomic interactions are further analyzed by calculating the valence electronic charge density distribution in two crystallographic planes. The semi-classical Boltzmann theory as incorporated in BoltzTraP code was used to calculate the transport properties of $Ba_2Cd_2As_3$ and $Ba_2Cd_2Sb_3$ at different temperatures and chemical potentials to ascertain the influence of temperatures and substituting As by Sb on the transport properties. The carries mobility decreases with increasing the temperature also with increasing the carriers concentration. We have observed that substituting As by Sb lead to increase the carries mobility of $Ba_2Cd_2Sb_3$ along the whole temperature interval and the carries concentration range. It has been found that $Ba_2Cd_2As_3$ exhibit higher carriers concentration, electronic electrical conductivity and Seebeck coefficient than that of $Ba_2Cd_2Sb_3$ along the investigated temperature range. The highest value of Seebeck coefficient occurs at 300 K, which show good agreement with the experimental data. The power factor increases linearly with increasing the temperature and $Ba_2Cd_2As_3$ exhibit a bit higher power factor than that of $Ba_2Cd_2Sb_3$ up to 500 K. Above this temperature both compounds are alternating. Based on the results our finding that the $Ba_2Cd_2Pn_3$ (Pn = As and Sb) compounds are efficient materials for energy conversion.

1. Introduction

Zintl phases are compounds that have shown promise for thermoelectric applications [1–6] and unusual properties [7–10]. Edward Zintl pioneered a new class of intermetallic compounds called Zintl phases, which constitute a large class of inorganic materials with very various crystal structures [11]. Since the discovery of the Zintl phases a large number of new Zintl compounds have been synthesized, and their structural and electronic characterizations have given tremendous information about their structure property relationship [12–20]. It has been found that in Zintl phase the nature of the chemical bonding can be understood by assuming a complete transfer of electrons from the more electropositive metal to the more electronegative element [21,22]. Due to their complex structure, Zintl phases have been classified as promising candidates for thermoelectric applications. Their electronic structure enable favorable thermal conductivity and the optimal charge transport properties [23,24]. Among the new promising Zintl phases are $Ba_2Cd_2As_3$ and $Ba_2Cd_2Sb_3$. Recently, these two compounds have been synthesized and characterized by Saparov et al. [15,16]. They reported that these compounds crystallize in a novel monoclinic structure with the space group C2/m featuring polyanionic layers made of Cd Pn_4 tetrahedra (Pn = As or Sb) and homoatomic Pn–Pn bonds.

* New Technologies - Research Centre, University of West Bohemia, Univerzitni 8, 306 14 Pilsen, Czech Republic
E-mail address: maalidph@yahoo.co.uk.

http://dx.doi.org/10.1016/j.jallcom.2016.02.010
0925-8388/

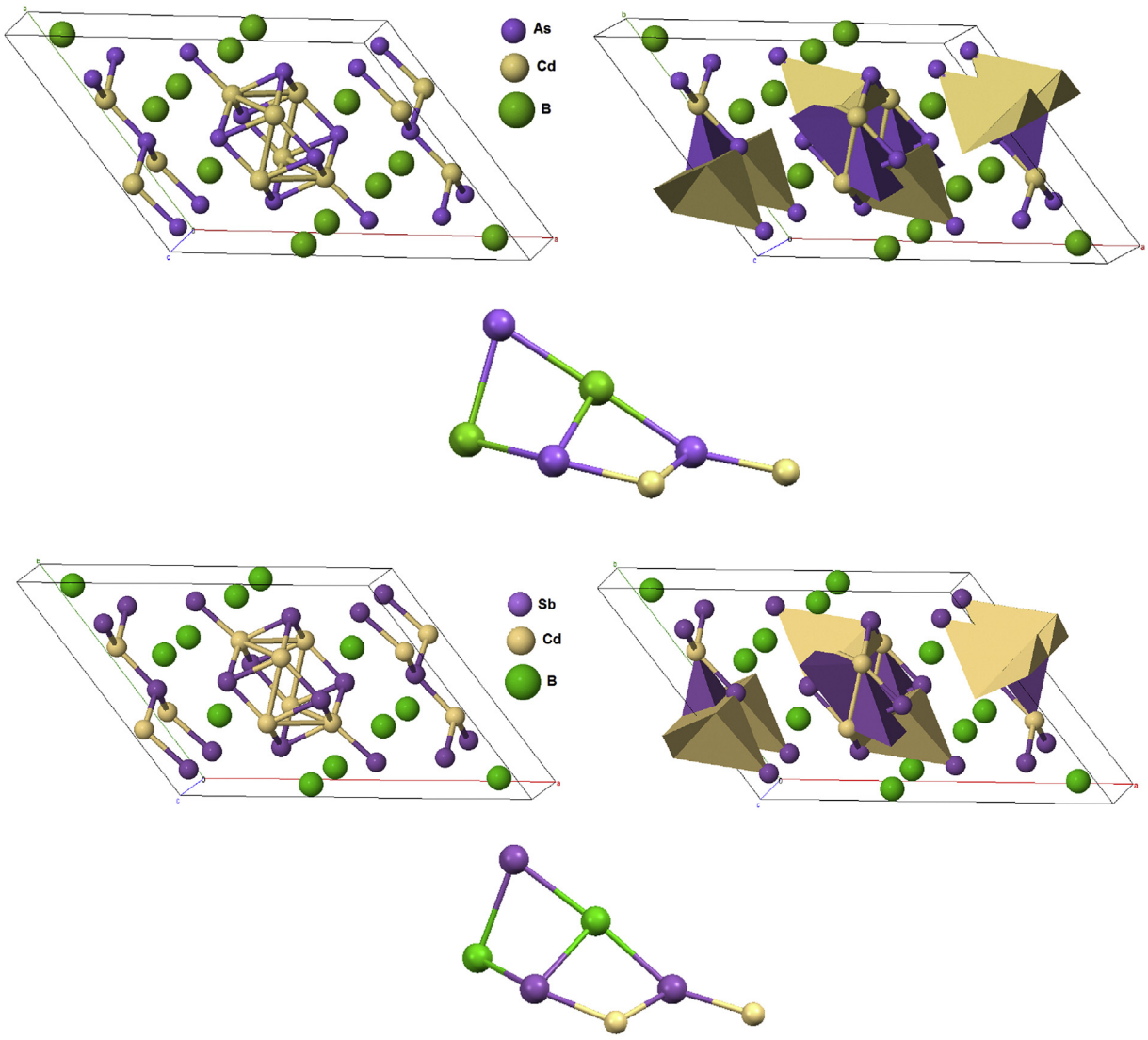

Fig. 1. The crystal structure of $Ba_2Cd_2As_3$ and $Ba_2Cd_2Sb_3$ compounds, which contains Sb_2 dimer and two Ba^{2+} cations.

Due to dearth information regarding the electronic structure and the transport properties of $Ba_2Cd_2Pn_3$ (Pn = As and Sb) compounds and due to the unique structure of these compounds [15,16,25,26], as well as the underestimation of the band gap of $Ba_2Cd_2Sb_3$ by the TB-LMTO-ASA calculation. Therefore, we thought it is worthwhile to perform comprehensive theoretical calculation based on the density functional theory within the recently modified Becke-Johnson potential (*mBJ*) [27] to investigate the electronic band structure, density of states, electronic charge density distribution and the thermoelectric properties. The thermoelectric properties were investigated at different temperatures and chemical potentials using BoltzTraP code [28] based on the calculated electronic structure to ascertain the effect of the temperatures on the thermoelectric properties. It has been proven that the first-principles calculation is a strong and useful tool to predict the crystal structure and its properties related to the electron configuration of a material before its synthesis [29–32].

2. Details of calculation

$Ba_2Cd_2Pn_3$ (Pn = As or Sb) crystallizes in Zintl phases with monoclinic space group $C2/m$, it contains two Ba, two Cd and three As or Sb atoms situated in special positions (symmetry independent) [15,16]. The lattice parameters of $Ba_2Cd_2As_3$ are a = 17.188(2) Å, b = 4.572(4) Å, c = 12.725(1) Å, β = 126.639(1)°, V = 798.0(1) Å^3 and ρ_c/g cm^{-1} = 6.028. While for $Ba_2Cd_2Sb_3$ are a = 18.072(4) Å, b = 4.824(1) Å, c = 13.403(3) Å, β = 126.747(2)°, V = 936.2(3) Å^3 and ρ_c/g cm^{-1} = 6.135 [15,16]. According to the Inorganic Crystal Structure Database [26], the atomic arrangement of these atoms make the structure of $Ba_2Cd_2Pn_3$ unique, it has two dimensional layers [15,16,25,26]. Based on the reported x-ray diffraction data (XRD) of $Ba_2Cd_2Pn_3$ (Pn = As or Sb) [15,16], a comprehensive theoretical calculation within density functional theory (DFT) was performed. The full potential linear augmented plane wave (*FPLAPW* + *lo*) method as embodied in the *WIEN2k* code [33] within generalized gradient approximation (*PBE–GGA*) [34] were used to perform the geometrical relaxation. The resulting relaxed geometries were used to calculate the electronic structure and hence the associated properties using the recently modified Becke-Johnson potential (*mBJ*) [27]. The relaxed crystal structures of $Ba_2Cd_2Pn_3$ (Pn = As or Sb) along with the asymmetric unit were presented in Fig. 1.

Based on the calculated electronic band structure of $Ba_2Cd_2As_3$ and $Ba_2Cd_2Sb_3$ compounds within full potential method, the semi-

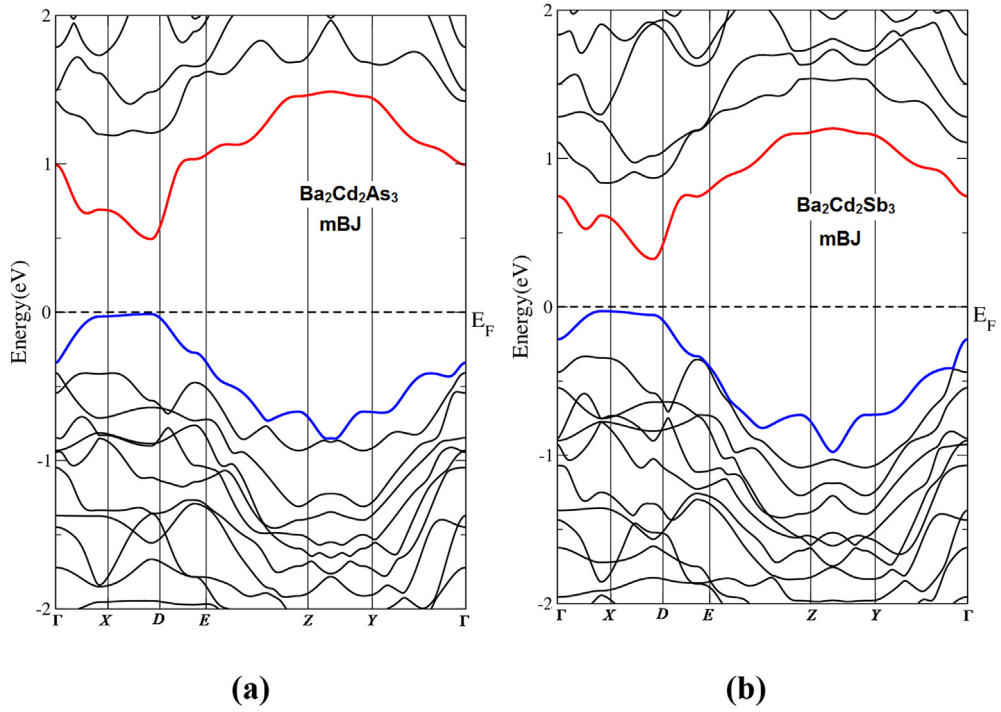

Fig. 2. Calculated electronic band structure of $Ba_2Cd_2As_3$ and $Ba_2Cd_2Sb_3$ compounds.

classical Boltzmann theory as incorporated in BoltzTraP code [28] was used to calculate the transport properties of $Ba_2Cd_2As_3$ and $Ba_2Cd_2Sb_3$ compounds at different temperatures and chemical potentials to ascertain the influence of temperatures and substituting As by Sb on the transport properties. In this report we have calculated the carriers concentration (n), Seebeck coefficient (S), electrical conductivity (σ/τ), electronic thermal conductivity (κ_e), and the electronic power factor ($S^2\sigma/\tau$) as a function of temperature at certain value of chemical potential as well as a faction of chemical potential at three constant temperatures (300, 600 and 900) K. We would like to mention here that the constant relaxation time approximation and the rigid band approximation are used in the calculations [28]. The relaxation time is taken to be direction independent and isotropic [35]. Madsen and Singh [28] have been reported that the BoltzTrap code depends on a well tested smoothed Fourier interpolation to obtain an analytical expression of bands. This is based on the fact that the electrons contributing to transport are in a narrow energy range due to the delta-function like Fermi broadening. For such a narrow energy range the relaxation time is nearly the same for the electrons. The accuracy of this method has been well tested earlier, and the method actually turns out to be a good approximation [36–39]. The temperature dependence of the energy band structure is ignored.

In the *FPLAPW + lo* calculation the unit cell was divided into two regions, the spherical harmonic expansion was used inside the non-overlapping spheres of muffin-tin radius (R_{MT}) and the plane wave basis set was chosen in the interstitial region (*IR*) of the unit cell. The R_{MT} for Ba, Cd, As and Sb were chosen in such a way that the spheres did not overlap, these values are 2.5 a.u for Ba, Cd, Sb and 2.3 a.u. for As. In order to get the total energy convergence, the basis functions in the *IR* were expanded up to $R_{MT} \times K_{max} = 7.0$ and inside the atomic spheres for the wave function. The maximum value of $\boldsymbol{l}$ was taken as $\boldsymbol{l}_{max} = 10$, while the charge density is Fourier expanded up to $G_{max} = 12$ (a.u)$^{-1}$. Self-consistency is obtained using 300 k points in the irreducible Brillouin zone (*IBZ*). The self-consistent calculations are converged since the total energy of the system is stable within 0.00001 Ry. The electronic band structures calculation are performed within 1500 k points in the *IBZ*. Whereas the transport properties are performed within 10,000 k points in the *IBZ*.

3. Results and discussion

3.1. Electronic band structures, density of states and electronic charge density

It has been reported that there are no other reported compounds with the same arrangement of $Ba_2Cd_2Pn_3$ (Pn = As or Sb) [15,16,25,26]. Therefore, it is very interesting to investigate the structure of such unique compounds. The electronic band structure of the monoclinic $Ba_2Cd_2As_3$ and $Ba_2Cd_2Sb_3$ compounds were calculated within the recently modified Becke-Johnson potential as shown in Fig. 2(a) and (b). Calculation explored that these compounds are narrow band gap semiconductors. It has been found that $Ba_2Cd_2As_3$ possess direct band gap of about 0.49 eV, whereas $Ba_2Cd_2Sb_3$ exhibit indirect band gap of about 0.32 eV. This finding confute the previous observation using TB-LMTO-ASA method, that $Ba_2Cd_2Sb_3$ is poor metal [15,16]. The drawback of TB-LMTO-ASA method is attributed to the fact that the muffin-tin approximation (MTA) works reasonably well in highly coordinated systems, such as face-centered cubic (FCC) metals. For covalently bonded solids or layered structures the MTA is a poor approximation and leads to discrepancies with experiments [40,41]. The more general treatment of the potential, such as provided by a full potential method has none of the drawbacks of the atomic sphere approximation (ASA) and MTA based methods. In full potential methods the potential and charge density are expanded into lattice harmonics inside each atomic sphere and as a Fourier series in the interstitial region. Hence, the effect of the full potential on the electronic properties can be ascertained. Following Fig. 2(a) and (b) it is clear that there are subtle difference in band desperations of the two compounds, resulting in significant influence on the

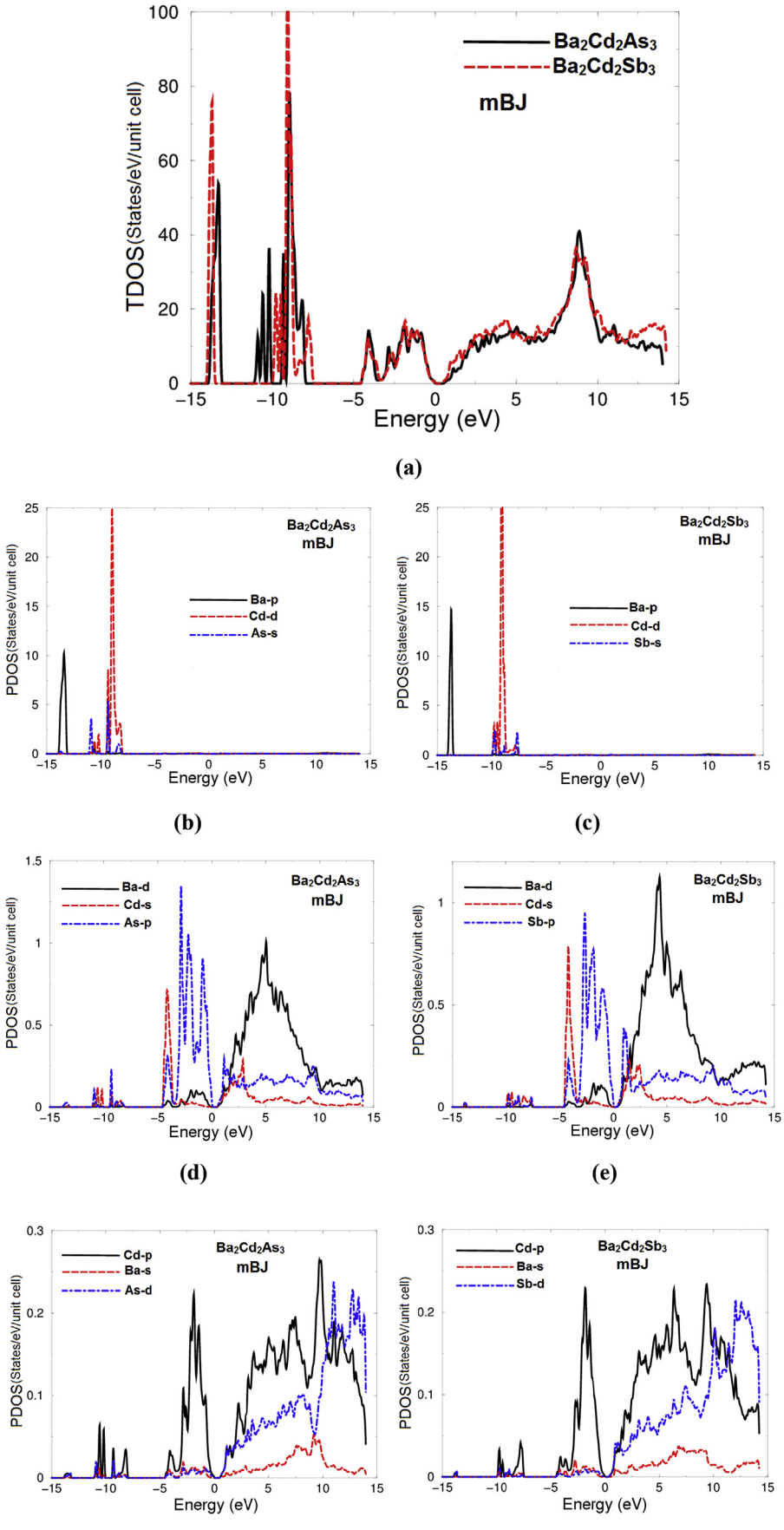

Fig. 3. Calculated total and partial density of states of $Ba_2Cd_2As_3$ and $Ba_2Cd_2Sb_3$ compounds.

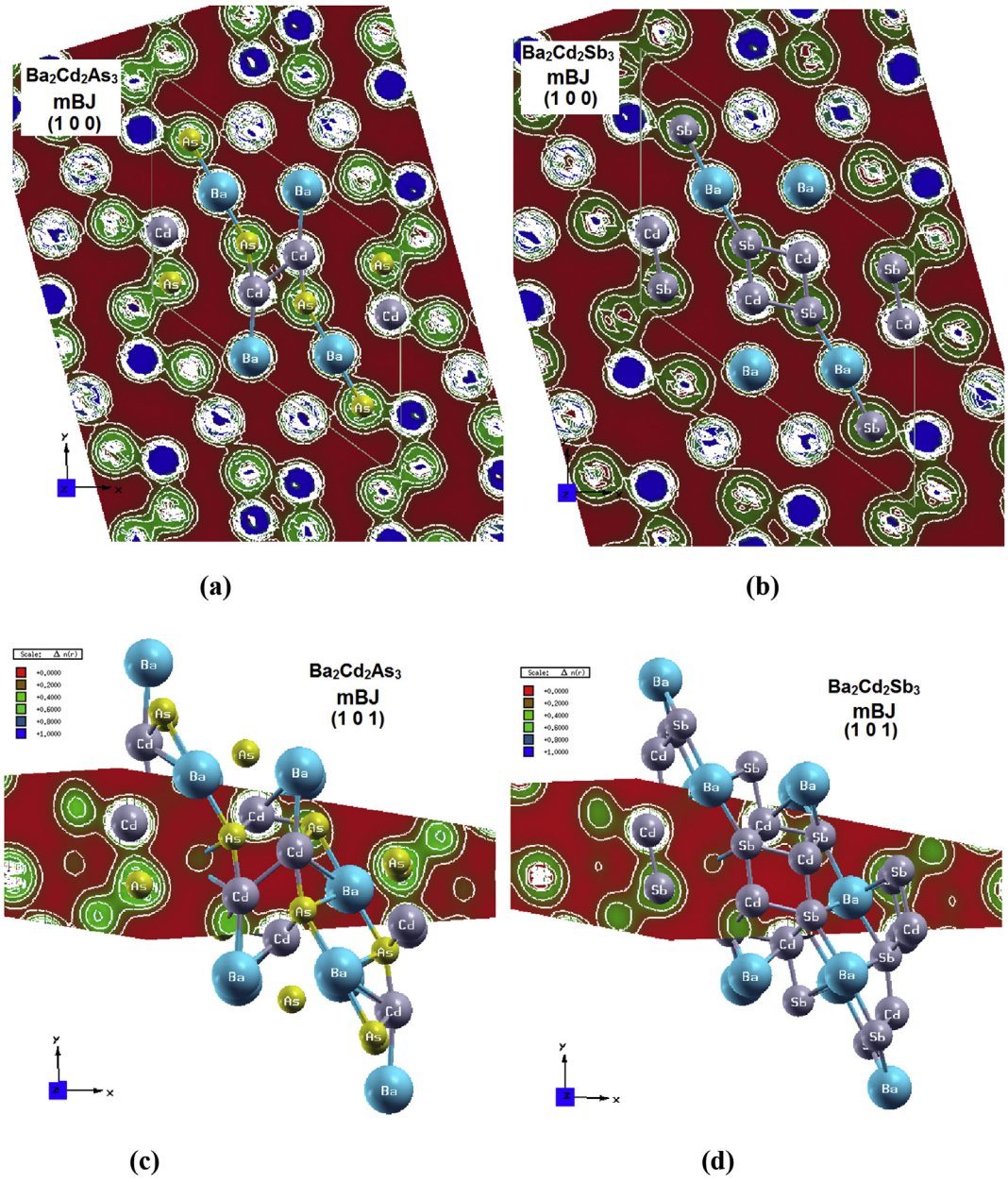

Fig. 4. Calculated electronic charge density counters; (a) illustrated the electronic charge density contour in (1 0 0) crystallographic plane for $Ba_2Cd_2As_3$; (b) illustrated the electronic charge density contour in (1 0 0) crystallographic plane for $Ba_2Cd_2Sb_3$; (c) illustrated the electronic charge density contour in (1 0 1) crystallographic plane for $Ba_2Cd_2As_3$; (d) illustrated the electronic charge density contour in (1 0 1) crystallographic plane for $Ba_2Cd_2Sb_3$.

electronic properties, taking into account the size and the electro-negativity differences between As and Sb. It is well known that substituting As by Sb lead to increase the inter-atomic distance, also cause to push the conduction band minimum (CBM) towards Fermi level (E_F), which could be another factor influence the electronic properties in addition to the influence of the electro-negativity differences.

To inspect the inter-atomic interactions, deep investigation to the total and the angular momentum resolved projected density of states were performed. Fig. 3(a) illustrated the total density of states (TDOS) of both compounds. We observed that $Ba_2Cd_2As_3$ introduced more bands in the energy region confined between −12.0 and −8.0 eV in comparison to $Ba_2Cd_2Sb_3$ due to the electro-negativity differences [42]. The calculated angular momentum resolved projected density of states (PDOS) enables us to identify the angular momentum characters of the various structures as shown in Fig. 3(b)-(g). These figures suggested that the density of states can be divided into four regions. The structure around −14.0 eV is mainly belong to Ba-p state with negligible contributions from Cd-s/p, As/Sb-p/d and Ba-s states. The second structure between −12.0 and −8.0 eV is formed by Cd-d and As/Sb-s states with small contribution of Cd-s/p, As/Sb-p/d and Ba-s states. The structure extended from −4.0 eV up to E_F is formed by Cd-s and As/Sb-p states with insignificant contribution from Ba-s/d, Cd-p and As/Sb-d states. The last structure, from the CBM and above is admixture of Ba-s/d, Cd-s/p and As/Sb-p/d states. There exists a strong hybridization between the states, at around −10.0 eV the Cd-d state hybridized with As/Sb-s states, at around −5.0 eV the Cd-s state hybridized with As/Sb-p states. At CBM the Cd-s state hybridized with As/Sb-p and Ba-d states while

Table 1
Calculated bond distance in comparison with the measured one [15,16].

$Ba_2Cd_2As_3$			$Ba_2Cd_2Sb_3$		
Bonds (Å)	Exp.	This work	Bonds (Å)	Exp.	This work
Ba1−As3	3.2451(6)	3.2121	Ba1−Sb3	3.4394(9)	3.4400
Ba1−As3 × 2	3.2798(4)	3.2699	Ba1− Sb3 × 2	3.4436(6)	3.4501
Ba1−As2	3.2932(6)	3.3011	Ba1−Sb2	3.4524(8)	3.4511
Ba1−As1 × 2	3.3426(5)	3.3487	Ba1−Sb1 × 2	3.4940(6)	3.5011
Ba2−As2 × 2	3.3586(4)	3.3499	Ba2−Sb2 × 2	3.5313(7)	3.5301
Ba2−As2	3.3780(6)	3.3798	Ba2−Sb2	3.5904(9)	3.6011
Ba2−As1 × 2	3.3884(4)	3.3900	Ba2−Sb1 × 2	3.5988(7)	3.6077
Ba2−As1 × 2	3.4992(5)	3.5010	Ba2−Sb1 × 2	3.7249(8)	3.7312
Ba2−Cd1 × 2	3.5932(4)	3.6000	Ba2−Cd1 × 2	3.6959(8)	3.7011
Cd1−As2	2.7151(6)	2.7099	Cd1−Sb2	2.901(1)	2.9000
Cd1−As3 × 2	2.7251(4)	2.7211	Cd1−Sb3 × 2	2.8853(6)	2.8987
Cd1−As1	2.8707(6)	2.8798	Cd1−Sb1	2.9712(9)	2.9800
Cd2−As3	2.7193(6)	2.7201	Cd2−Sb3	2.8794(9)	2.8811
Cd2−As3 × 2	2.7347(4)	2.7355	Cd2−Sb3 × 2	2.9029(6)	2.9111
Cd2−As3	2.9093(7)	2.9111	Cd2−Sb3	3.0403(9)	3.0344
As1−As1	2.498(1)	2.4968	Sb1−Sb1	2.835(1)	2.8400
As1−Cd1	2.8707(6)	2.8877	Sb1−Cd1	2.9712(9)	2.9811
As2−Cd1	2.7151(6)	2.7090	Sb2−Cd1	2.901(1)	2.9011
As2−Cd2 × 2	2.7347(4)	2.7400	Sb2−Cd2 × 2	2.9029(6)	2.9112
As3−Cd2	2.7193(6)	2.7211	Sb3−Cd2	2.8794(9)	2.8866
As3−Cd1 × 2	2.7251(4)	2.7233	Sb3−Cd1 × 2	2.8853(6)	2.8900
As3−Cd2	2.9093(7)	2.8998	Sb3−Cd2	3.0403(9)	3.0411

Cd-p state hybridized with As/Sb-d states, these states are govern the value of the band gap mainly the As/Sb-p states which are the dominant in the CBM and the valence band maximum (VBM). This finding confute the previous observation using TB-LMTO-ASA method that the classical sp^3 hybridization concept for CdPn_4 tetrahedra is inapplicable in $Ba_2Cd_2As_3$ and $Ba_2Cd_2Sb_3$ [15,16]. The strong hybridization may lead to form covalent bonding. Covalent bonding is more favorable for the transport of the carriers than ionic one [43].

To support this statement, deep insight into the electronic structure and the inter-atomic interactions will be obtained by analyzing the valence electronic charge density distribution (VECD). Therefore, we have investigated the VECD in two crystallographic planes. These are (1 0 0) and (1 0 1) as shown in Fig. 4(a)–(d). The nature of the inter-atomic interactions in $Ba_2Cd_2Pn_3$ (Pn = As or Sb) compounds could be understood by assuming a complete transfer of electrons from the more electropositive metal (here Ba and Cd) to the more electronegative element (As and Sb). According to Pauling scale the electronegativity of As and Sb are 2.18 and 2.05, whereas the electronegativity of Ba and Cd are 0.89 and 1.69 thus Ba and Cd possess high electropositivity of about 3.11 and 2.31. Therefore, they are similar to the typical semiconductors [15,16]. Due to the atomic radii differences, substituting As by Sb lead to increase the inter-atomic distance which influence the degree of covalency between Ba–Pn (Pn = As or Sb) [15,16] and Cd-Pn. Following Fig. 4(a) and (b) it is clear that Cd-Pn form partially ionic and partially covalent bonding implies the existence of the hybridization, while Ba-Pn exhibit mostly ionic and partially covalent bonding and substituting As by Sb lead to influence degree of covalency, as it is clear from Fig. 4(b) where the sharing contour (outer shell) between Ba–Sb about to vanishes in comparison to Ba–As. To investigate the anisotropy nature of the bonds in $Ba_2Cd_2Pn_3$ (Pn = As or Sb) we have calculated the VECD in (1 0 1) crystallographic plane as shown in Fig. 4(c) and (d), the anisotropy could be confirmed further by calculating inter-atomic distances. These are listed in Table 1 in comparison with measured one [15,16]. In addition, the bond angles were calculated and compared with the measured one as shown in Table 2. Due to electro-negativity differences between Ba, Cd, As and Sb atoms we can see that the charge attracted towards As or Sb atoms due to the fact that a complete transfer of electrons from the more electropositive metal to the more electronegative element.

3.2. Thermoelectric properties

It is well known that the area in vicinity of Fermi level (E_F) play an important rule for the carrier's transportation therefore, we have illustrated the electronic band structures in the energy ranges between +2.0 eV and −2.0 eV as shown in Fig. 2(a) and (b). It is clear that the upper valence band (Fig.2(a,b)) shows flat k-dispersion. This reflects the low mobility of the holes. Whereas the lower conduction band exhibit highest k-dispersion which imply lowest effect masses and hence the highest mobility for the electrons. The calculated electron effective mass (m_e^*) and effective mass ratio (m_e^*/m_e) of $Ba_2Cd_2As_3$ are 0.0617×10^{-31} kg and 0.0067, while for $Ba_2Cd_2Sb_3$ are 0.0539×10^{-31} kg and 0.0059. Since the investigated compounds possess narrow energy gaps. Therefore, the electronic structures of these compounds allow the optimal charge transport properties.

3.2.1. Charge carriers concentration and electrical conductivity

We have calculated the carries mobility of $Ba_2Cd_2As_3$ and $Ba_2Cd_2Sb_3$ compounds at a certain value of the chemical potential as a function of temperature as shown in Fig. 5(a) also as a function of carriers concentration as illustrated in Fig. 5(b). It has been found that the carries mobility decreases with increasing the temperature (Fig. 5(a)). The same behaviors was observed with increasing the carriers concentration (Fig. 5(b)), that is attributed to the fact that high temperature lead to increase the vibration resulting in dramatically increase the scattering rate and hence reduce the mobility. The same trends observed with increasing the carriers concentration. That means the high carriers concentration increase the scattering rate resulting in reduce the mobility. Also we observed that substituting As by Sb in $Ba_2Cd_2Pn_3$ (Pn = As and Sb) lead to increase the carries mobility of $Ba_2Cd_2Sb_3$ along the whole temperature scale with respect to $Ba_2Cd_2As_3$ (see Fig. 5(a)) also it cause to increase the carries mobility of $Ba_2Cd_2Sb_3$ along the carries

Table 2
Calculated bond angles in comparison with the measured one [15,16].

$Ba_2Cd_2As_3$			$Ba_2Cd_2Sb_3$		
Bond angles (°)	Exp.	This work	Bond angles (°)	Exp.	This work
As2−Cd1−As3	107.31(1)	107.35	Sb2−Cd1−Sb3	105.78(2)	105.89
As3−Cd1−As3	113.09(2)	113.1	Sb3−Cd1−Sb3	113.43(3)	113.51
As1−Cd1−As2	109.54(2)	109.6	Sb1−Cd1−Sb2	112.59(3)	112.61
As1−Cd1− As3	109.75(1)	109.70	Sb1−Cd1−Sb3	109.61(2)	109.59
As2−Cd2−As2	112.49(2)	112.51	Sb2−Cd2−Sb2	112.38(3)	112.30
As3−Cd2−As3	111.06(2)	111.1	Sb3−Cd2−Sb3	109.90(2)	109.87
	114.11(1)	114.15		114.61(2)	114.56
As3−Cd2−As2	101.81(1)	101.75	Sb3−Cd2−Sb2	101.85(2)	101.79

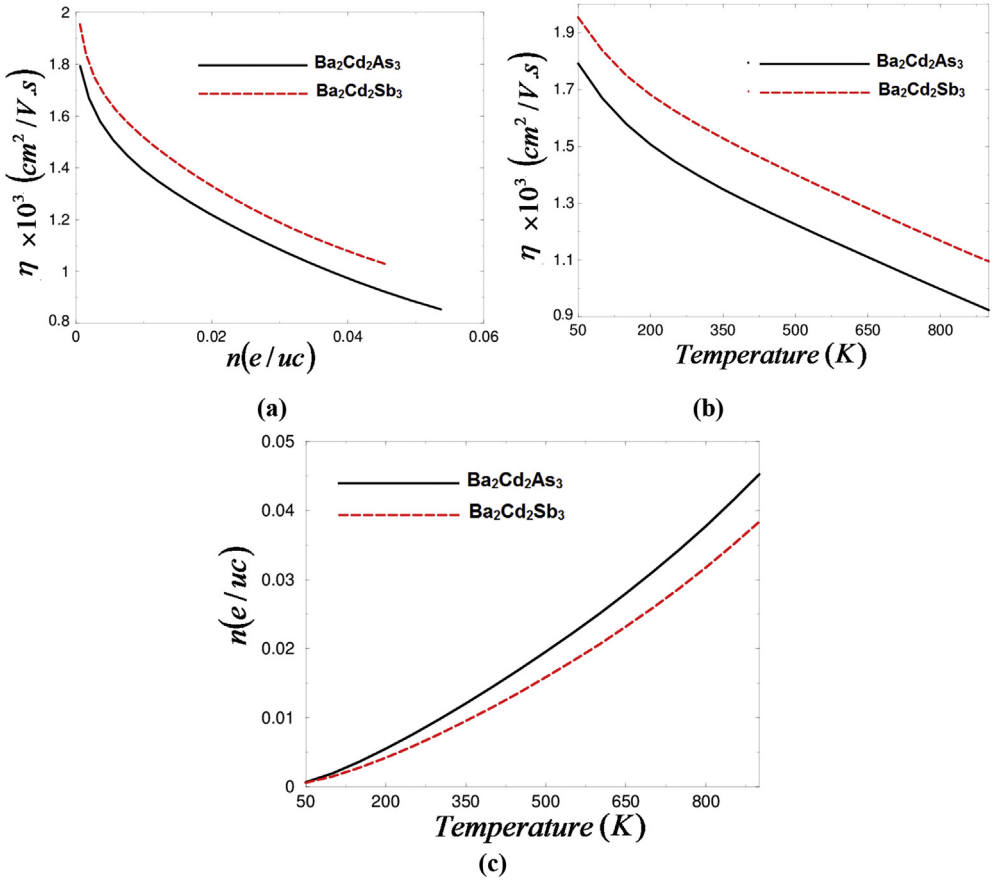

Fig. 5. (a) Calculated mobility as function of temperature at a certain value of chemical potential; (b) Calculated mobility as function of carriers concentration at a certain value of chemical potential; (c) Calculated carriers concentration as function of temperature at a certain value of chemical potential.

concentration range in comparison to $Ba_2Cd_2As_3$ (see Fig. 5(b)).

In addition, we have calculated and presented the charge carriers concentration of $Ba_2Cd_2Pn_3$ (Pn = As and Sb) compounds at certain value of chemical potential ($\mu = E_F$) as a function of temperature as shown in Fig. 5(c). Following this figure we can see that at this certain value of the chemical potential a rapid increases in the carrier concentration of these compounds occurs with increasing the temperature. $Ba_2Cd_2As_3$ compound exhibit higher values than that of $Ba_2Cd_2Sb_3$ compounds along the investigated temperature range. That is attributed to the fact that the electronegativity of As is a bit higher than that of Sb and due to the fact that a complete transfer of electrons occurs from the more electropositive metal (here Ba > Cd) to the more electronegative element (As > Sb). The carrier concentration ($n = \sigma/e\eta$) is indirectly related to the effective mass through the mobility ($\eta_e = e\tau_e/m_e^*$) since m_e^* of $Ba_2Cd_2As_3$ > $Ba_2Cd_2Sb_3$ therefore, the η of $Ba_2Cd_2As_3$ < $Ba_2Cd_2Sb_3$ (Fig. 5(a,b)) and hence n of $Ba_2Cd_2As_3$ > $Ba_2Cd_2Sb_3$ (Fig. 5(c)).

Fig. 6(a) illustrated the electrical conductivity as a function of temperature at a certain value of chemical potential. It has been noticed that the electrical conductivity increases linearly with increasing the temperature and $Ba_2Cd_2As_3$ compound exhibit electrical conductivity a bit higher or almost equal to that of $Ba_2Cd_2Sb_3$ compound. We have compared our results of $Ba_2Cd_2As_3$ with the experimental data [15], good agreement was found see Fig. S1 (supplementary materials). The electrical conductivity ($\sigma = ne\eta$) is directly proportional to the charge carriers density (n) and their mobility (η) therefore, to have the highest electrical conductivity, high $n\eta$ is required thus we have to maximizing the quantity $n\eta$. Since $Ba_2Cd_2As_3$ possess high n and a bit low η while $Ba_2Cd_2Sb_3$ have low n and a bit high η therefore, $n\eta$ of $Ba_2Cd_2As_3 \geq$ $Ba_2Cd_2Sb_3$ as shown in Fig. 6(a) and Fig. S1 (supplementary materials).

Furthermore, we have plotted the electrical conductivity as a function of chemical potential at three constant temperatures (300, 600 and 900) K as shown in Fig. 6(b) and (c). These figures confirm our previous finding that in the vicinity of E_F the electrical conductivity of $Ba_2Cd_2As_3 \geq$ $Ba_2Cd_2Sb_3$. We observed that increasing the temperature has no significant influence on the electrical conductivity in the investigated chemical potential range.

3.2.2. Electronic thermal conductivity

For ideal thermoelectric materials low thermal conductivity is required to maintain the temperature gradient. In general the thermal conductivity consist of two parts $\kappa = \kappa_e + \kappa_l$, the first part κ_e which defined the electronic contribution where both of electrons and holes transporting heat, and the second part κ_l is the lattice contribution (phonons traveling through the lattice). Using the Boltztrap code we have calculated the temperature dependent electronic thermal conductivity of $Ba_2Cd_2As_3$ and $Ba_2Cd_2Sb_3$ compounds at a certain value of the chemical potential as shown in Fig. 7(a). It has been noticed that the electronic thermal conductivity increases exponentially with the temperature and both compounds exhibit the same values up to 550 K. Above this temperature $Ba_2Cd_2Sb_3$ show higher electronic thermal conductivity than that of $Ba_2Cd_2As_3$. In addition, we have calculated the electronic thermal conductivity as a function of chemical potential in the vicinity of E_F for three constant temperatures as shown in

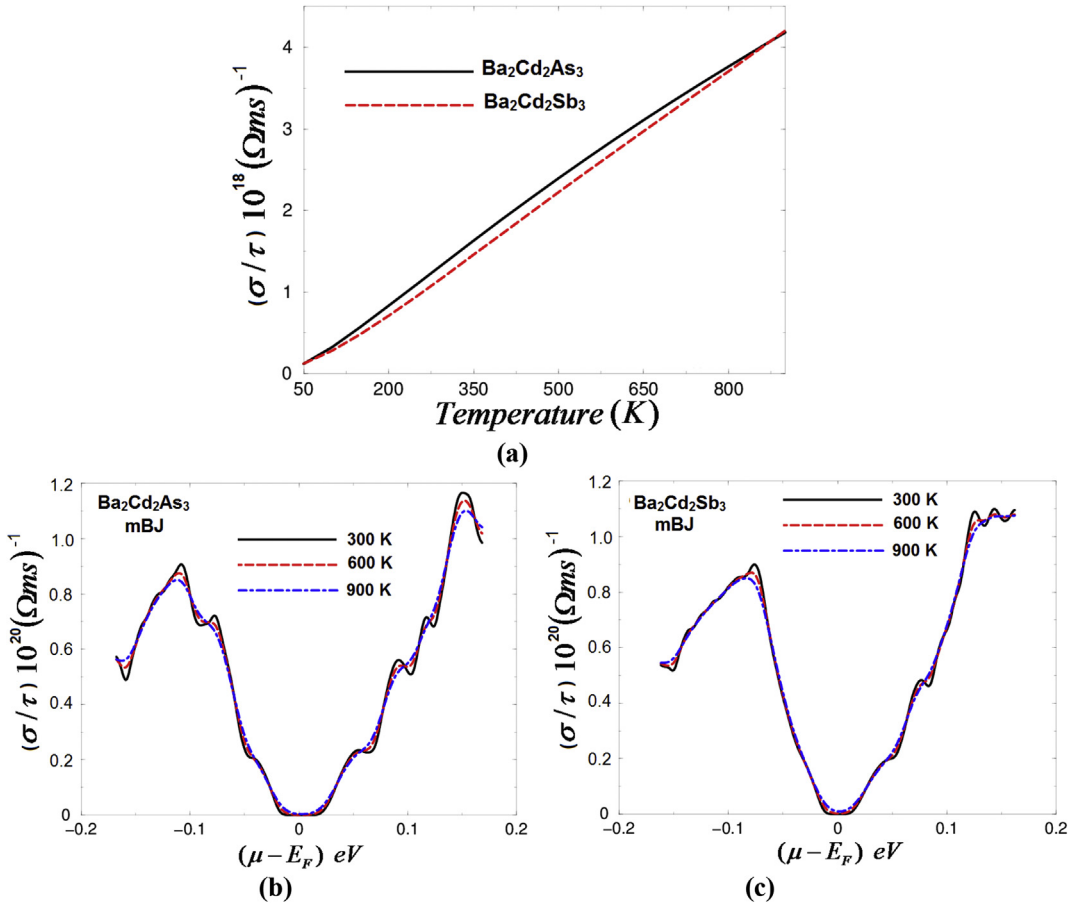

Fig. 6. (a) Calculated electrical conductivity of $Ba_2Cd_2Pn_3$ (Pn = As and Sb) compounds using mBJ as a function of temperatures; (b) Calculated electrical conductivity of $Ba_2Cd_2As_3$ as a function of chemical potential at three constant temperatures 300, 600 and 900 K; (c) Calculated electrical conductivity of $Ba_2Cd_2Sb_3$ as a function of chemical potential at three constant temperatures 300, 600 and 900 K.

Fig. 7(b) and (c). A significant increases in the electronic thermal conductivity occurs with increasing the temperature from 300 → 600 → 900 K. The lowest electronic thermal conductivity is achieved at 300 K for the investigated compounds.

3.2.3. Seebeck coefficient (thermopower)

Fig. 8(a) and (b) illustrated the calculated Seebeck coefficient (S) as a function of chemical potential in the interval range $\mu - E_F = \mp 0.2$ eV, at three constant temperatures (300, 600 and 900) K. It has been found that in the investigated interval of the chemical potential, both of $Ba_2Cd_2As_3$ and $Ba_2Cd_2Sb_3$ compounds represent n-type and p-type conductions. $Ba_2Cd_2As_3$ exhibit higher Seebeck coefficient than $Ba_2Cd_2Sb_3$ compound for all temperatures and the highest value of Seebeck coefficient occurs at 300 K. In Fig. S2 (supplementary materials) we have plotted the Seebeck coefficient of $Ba_2Cd_2As_3$ as a function of temperature up to 300 K along with the experimental data [16], same trends was found confirming the validity of the method used. It is clear that at the vicinity of Fermi level there are two pronounced peaks represents Seebeck coefficient for n-/p-types of $Ba_2Cd_2As_3$ and $Ba_2Cd_2Sb_3$ compounds. We can see that $Ba_2Cd_2As_3$ exhibit the highest values of about 840.0 ($\mu V/K$) for p-type and 790.0 ($\mu V/K$) for n-type conductions. While $Ba_2Cd_2Sb_3$ compound exhibits the maximum values of about 560.0 ($\mu V/K$) for p-type and 510.0($\mu V/K$) for n-type conductions.

3.2.4. Power factor

The most challenging task is to increase the dimensionless figure of merit ($ZT = S^2\sigma T/k$). To achieve this task we need to maximizing the quantity $S^2\sigma$ and to minimize k. Therefore, we need materials exhibit low thermal conductivity and high power factor $P = S^2\sigma$. The power factor comes as numerator of the dimensionless figure of merit and hence the power factor is an important quantity which play principle role in evaluate the transport properties of the materials.

Fig. 9(a) exhibit the calculated P of $Ba_2Cd_2As_3$ and $Ba_2Cd_2Sb_3$ compounds as a function of temperature at certain value of chemical potential. It is clear that the power factor increases linearly with increasing the temperature and $Ba_2Cd_2As_3$ exhibit a bit higher power factor than that of $Ba_2Cd_2Sb_3$ up to 500 K. Above this temperature both compounds are alternating.

In Fig. 9(b) and (c) we have presented the calculated power factor of $Ba_2Cd_2As_3$ and $Ba_2Cd_2Sb_3$ compounds at 300, 600 and 900 K as a function of chemical potential at the vicinity of E_F for $\mu - E_F$ between ±0.2 eV. At $\mu - E_F = 0$ the power factor exhibit low value and beyond that the power factor increases rapidly to form pronounced peaks. The power factor of $Ba_2Cd_2As_3$ exhibit the highest peaks for the p-type conduction at around $\mu - E_F = -0.04$ eV for 300, 600 and 900 K. While $Ba_2Cd_2Sb_3$ exhibit the highest peaks for the p-type conduction at around $\mu - E_F = -0.025$ eV. Both compounds the highest power factor occurs at 900 K.

4. Conclusions

Based on the reported x-ray diffraction data (XRD) of $Ba_2Cd_2Pn_3$

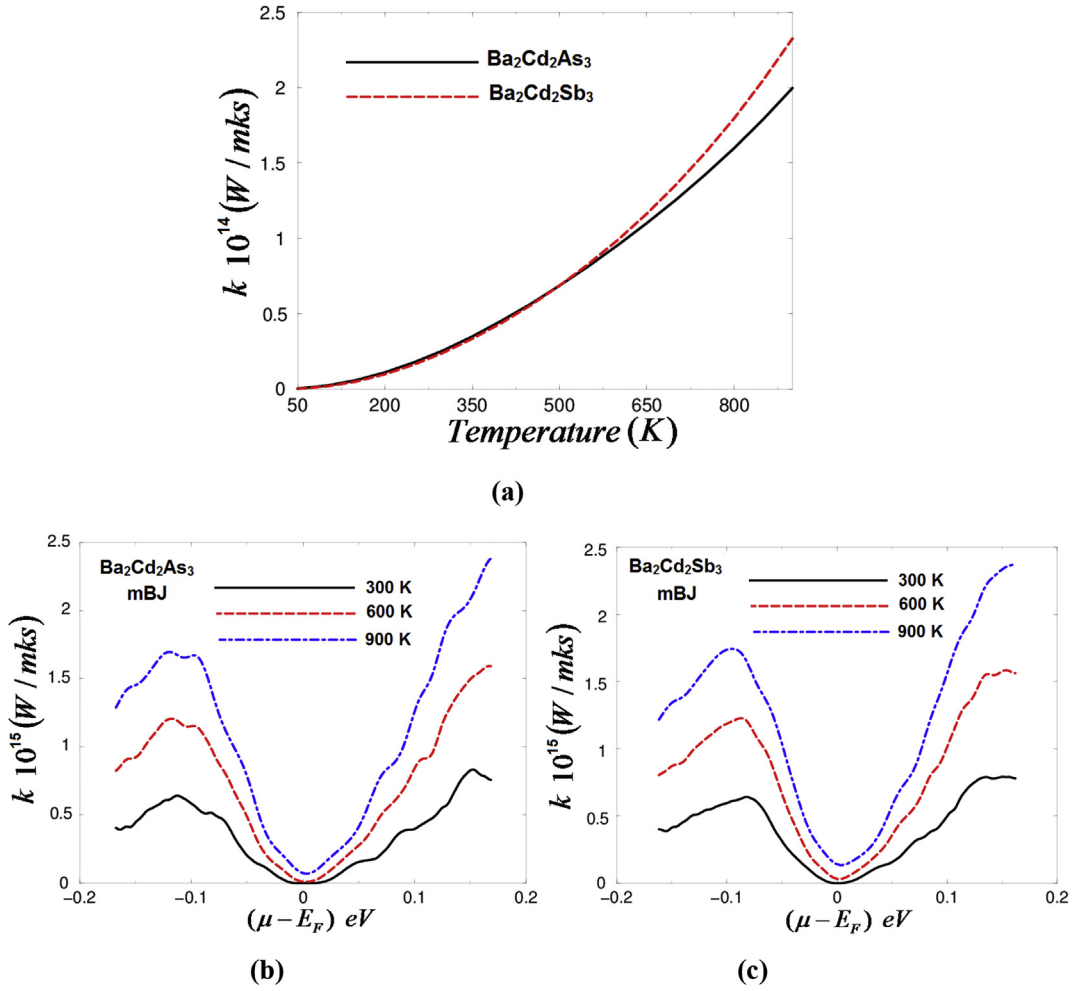

Fig. 7. (a) Calculated electronic thermal conductivity of $Ba_2Cd_2Pn_3$ (Pn = As and Sb) compounds as a function of temperatures; (b) Calculated electronic thermal conductivity of $Ba_2Cd_2As_3$ as a function of chemical potential at three constant temperatures 300, 600 and 900 K; (c) Calculated electronic thermal conductivity of $Ba_2Cd_2Sb_3$ as a function of chemical potential at three constant temperatures 300, 600 and 900 K.

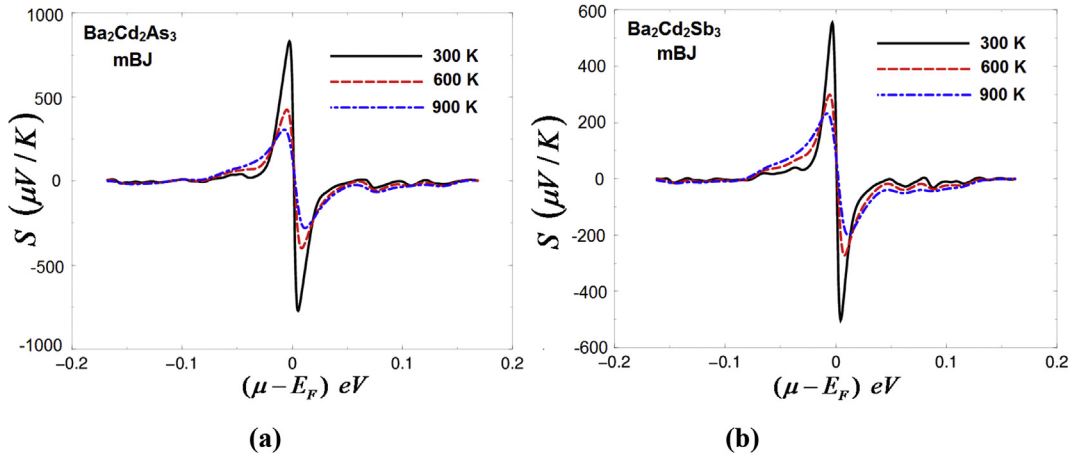

Fig. 8. (a) Calculated Seebeck coefficient of $Ba_2Cd_2As_3$ as a function of chemical potential at three constant temperatures 300, 600 and 900 K; (b) Calculated Seebeck coefficient of $Ba_2Cd_2Sb_3$ as a function of chemical potential at three constant temperatures 300, 600 and 900 K.

(*Pn* = As or Sb) a comprehensive theoretical calculation was performed. The full potential linear augmented plane wave (*FPLAPW* + *lo*) method within generalized gradient approximation (*PBE*−*GGA*) were used to perform the geometrical relaxation. The full potential method within the recently modified Becke-Johnson potential explore that the $Ba_2Cd_2Pn_3$ (*Pn* = As and Sb) compounds are narrow band gap semiconductors with subtle difference in band desperations of the two compounds. These differences

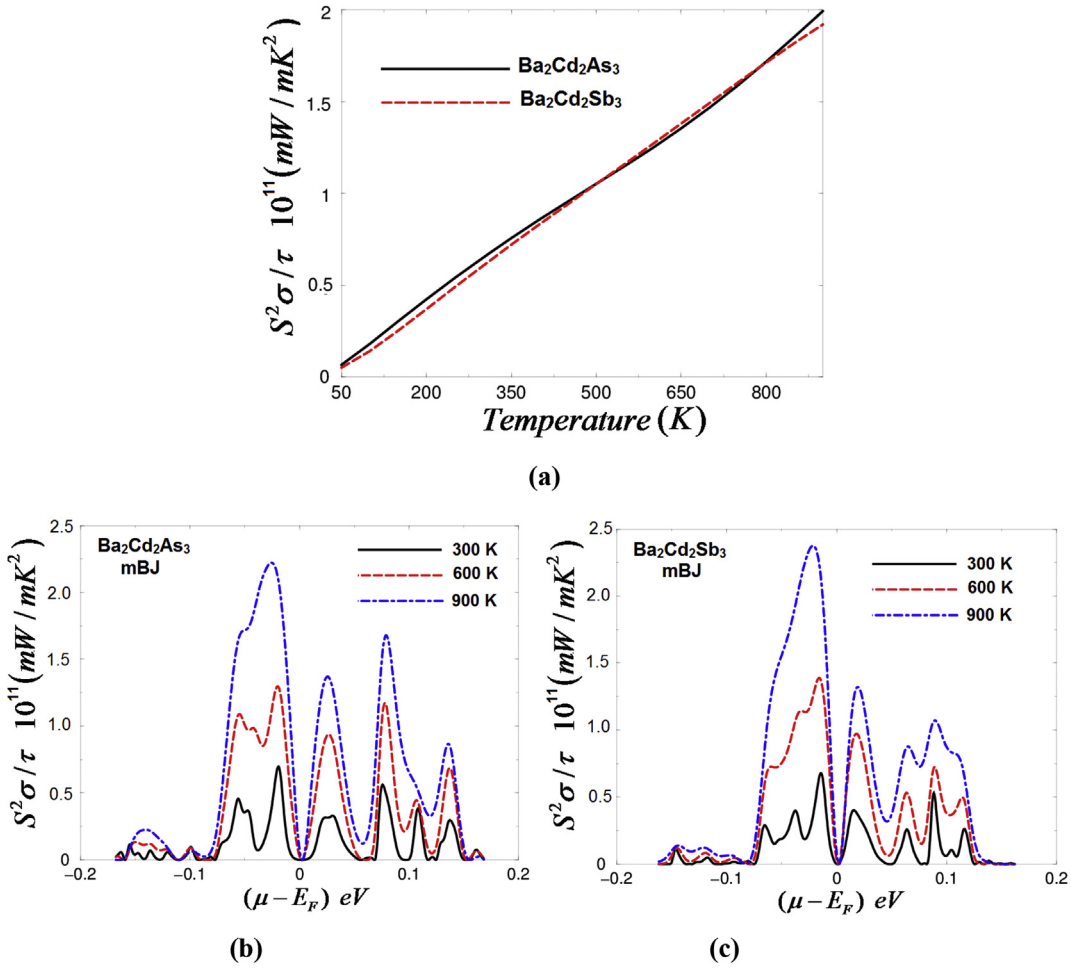

Fig. 9. (a) Calculated power factor of $Ba_2Cd_2Pn_3$ (Pn = As and Sb) compounds as a function of temperatures; (b) Calculated power factor of $Ba_2Cd_2As_3$ as a function of chemical potential at three constant temperatures 300, 600 and 900 K; (c) Calculated power factor of $Ba_2Cd_2Sb_3$ as a function of chemical potential at three constant temperatures 300, 600 and 900 K.

cause significant influence on the electronic properties of these materials, taking into account the size and the electro-negativity differences between As and Sb atoms. The calculated PDOS exhibit that there exists a strong hybridization between the states. The investigated valence electronic charge density distribution in two crystallographic planes explore further information about the electronic structure, anisotropy, the inter-atomic interactions and the chemical bonding nature. To get deep insight into the electronic structure, the optical properties were calculated and analyzed in details.

Based on the calculated band structure of $Ba_2Cd_2Pn_3$ (Pn = As and Sb), the transport properties were obtained using the semi-classical Boltzmann theory as incorporated in BoltzTraP code. To ascertain the influence of substituting As by Sb on the transport properties the investigations were achieved at different temperatures and chemical potentials values. Calculation show that these materials are narrow gap semiconductors and efficient materials for energy conversion.

The carries mobility decreases with increasing the temperature and the carries concentration. Substituting As by Sb in $Ba_2Cd_2Pn_3$ (Pn = As and Sb) lead to increase the carries mobility along the whole temperature range and the carries concentration range. It has been found that $Ba_2Cd_2As_3$ compound exhibit higher carriers concentration, electronic electrical conductivity, Seebeck coefficient and power factor than that of $Ba_2Cd_2Sb_3$ compounds along the investigated temperature range. The Seebeck coefficient of $Ba_2Cd_2As_3$ compound show good agreement with the available experimental data. The obtained results suggested that these compounds are good thermoelectric materials and $Ba_2Cd_2As_3$ compound is a bit better than $Ba_2Cd_2Sb_3$ compound due to the fact that As has a bit higher electronegativity than Sb and $Ba_2Cd_2As_3$ posses a direct band gap.

Some important notes

We would like to highlight that we have used (η) for mobility in order to differentiate it from the chemical potential (μ).

Acknowledgments

The result was developed within the CENTEM project, reg. no. CZ.1.05/2.1.00/03.0088, cofunded by the ERDF as part of the Ministry of Education, Youth and Sports OP RDI programme and, in the follow-up sustainability stage, supported through CENTEM PLUS (LO1402) by financial means from the Ministry of Education, Youth and Sports under the "National Sustainability Programme I. Computational resources were provided by MetaCentrum (LM2010005) and CERIT-SC (CZ.1.05/3.2.00/08.0144) infrastructures.

Appendix A. Supplementary data

Supplementary data related to this article can be found at http://dx.doi.org/10.1016/j.jallcom.2016.02.010.

References

[1] N. Kazem, W. Xie, S. Ohno, A. Zevalkink, G.J. Miller, G.J. Snyder, S.M. Kauzlarich, Chem. Mater 26 (2014) 1393–1403.
[2] J. Cooley, N. Kazem, J.V. Zaikina, J.C. Fettinger, S.M. Kauzlarich, Inorg. Chem. 54 (2015) 11767–11775.
[3] S. Xia, S. Bobev, J. Am, Chem. Soc. 129 (2007) 4049–4057.
[4] S.S. Stoyko, M. Khatun, A. Mar, Inorg. Chem. 51 (2012) 2621–2628.
[5] N. Kazem, J.V. Zaikina, S. Ohno, G.J. Snyder, S.M. Kauzlarich, Chem. Mater 27 (2015) 7508–7519.
[6] Y. Wang, S. Stoyko, S. Bobev, Inorg. Chem. 54 (2015) 1931–1939.
[7] B. Saparov, S. Bobev, Dalton Trans. 39 (2010) 11335–11343.
[8] B. Saparov, S. Bobev, Inorg. Chem. 49 (2010) 5173–5179.
[9] B. Saparov, S. Bobev, Acta Cryst. E67 (2011) i11.
[10] B. Saparov, M. Saito, S. Bobev, J. Solid State Chem. 184 (2011) 432–440.
[11] E. Zintl, Intermet. Verbindungen. Angew. Chem. 52 (1939) 1.
[12] J.D. Corbett, in: S.M. Kaurlarich (Ed.), Chemistry, Structure, and Bonding of Zintl Phases and Ions, VCH, New York, 1996, p. 139.
[13] J.D. Corbett, Diverse naked clusters of the heavy main-group elements. Electronic regularities and analogies, Struct. Bond. 87 (1997) 157–193.
[14] J.D. Corbett, Angew. Chem. Int. Ed. 39 (2000) 670–690.
[15] B. Saparov, H. Hua, X. Zhang, R. Greene, S. Bobev, Dalton Trans. 39 (2010) 1063–1070.
[16] http://www.rsc.org/suppdata/dt/b9/b914305j/b914305j.pdf.
[17] G.J. Miller, in: S.M. Kauzlarich (Ed.), Chemistry, Structure, and Bonding of Zintl Phases and Ions, VCH, New York, 1996, p. 1.
[18] B. Eisenmann, G. Cordier (4. S. M. Kauzlarich), in: Chemirtry, Structure and Bonding of Zintl Phases and Ions, VCH Publishers, Inc., New York, NY, 1996, p. 61.
[19] W. van der Lugt, in: S.M. Kauzlarich (Ed.), Chemistry, Shucture, and Bonding of Zintl Phases and Ions, VCH, New York, 1996, p. 183.
[20] C. Belin, M. Tillard-Charbonnel, Frameworks of clusters in alkali metal-gallium phases: structure, bonding and properties, Prog. Solid State Chem. 22 (1993) 59–109.
[21] E. Zintl, Angew. Chem. 52 (1939) 1. Chemistry, Structure, and Bonding of Zintl Phases and Ions, ed. S. M. Kauzlarich, VCH Publishers, New York, 1996.
[22] R. Nesper, Prog. Solid State Chem. 20 (1990) 1–45.
[23] G.J. Snyder, E.S. Toberer, Nat. Mater 7 (2008) 105–114.
[24] S.M. Kauzlarich, S.R. Brown, G.J. Snyder, Dalton Trans. (2007) 2099–2107.
[25] P. Villars, L.D. Calvert (Eds.), Pearson's Handbook of Crystallographic Data for Intermetallic Phases, second ed., ASM International, Materials Park, OH, 1991. P. Villars, Pearson's Handbook of Crystallographic Data for Intermetallic Phases, ASM International, Materials Park, OH, desktop edn., 1997.
[26] ICSD Database, Fachinformationszentrum, 2008. Karlsruhe, Germany.
[27] F. Tran, P. Blaha, Phys. Rev. Lett. 102 (2009) 226401.
[28] G.K.H. Madsen, D.J. Singh, Comput. Phys. Commun. 175 (2006) 67–71.
[29] K.J. Plucinski, I.V. Kityk, J. Kasperczyk, B. Sahraoui, Semicond. Sci. Technol. 16 (2001) 467–470.
[30] M. Malachowski, I.R. Kityk, B. Sahraoui, Phys. Lett. A 242 (1998) 337–342.
[31] I. Fuks-Janczarek, R. Miedzinski, M.G. Brik, A. Majchrowski, L.R. Jaroszewicz, I.V. Kityk, Solid State Sci. 27 (2014) 30–35.
[32] A.H. Reshak, A. Majchrowski, M. Swirkowicz, A. Kłos, T. Łukasiewicz, I.V. Kityk, K. Iliopoulos, S. Couris, M.G. Brik, J. Alloys Compd. 481 (2009) 14–16.
[33] P. Blaha, K. Schwarz, G.K.H. Madsen, D. Kvasnicka, J. Luitz, WIEN2k, an Augmented Plane Wave Plus Local Orbitals Program for Calculating Crystal Properties, Vienna University of Technology, Austria, 2001.
[34] J.P. Perdew, K. Burke, M. Ernzerhof, Phys. Rev. Lett. 77 (1996) 3865–3868.
[35] B. Xu, X. Li, G. Yu, J. Zhang, S. Ma, Y. Wang, L. Yi, J. Alloys Compd. 565 (2013) 22–28.
[36] D. Wang, L. Tang, M.Q. Long, Z.G. Shuai, J. Chem. Phys. 131 (2009) 224704.
[37] R. Chmielowski, D. Pere, C. Bera, I. Opahle, W. Xie, S. Jacob, F. Capet, P. Roussel, A. Weidenkaff, G.K.H. Madsen, G. Dennler, J. Appl. Phys. 117 (2015) 125103.
[38] H. Shi, D. Parker, D. Mao-Hua, D.J. Singh, Phys. Rev. Appl. 3 (2015) 014004.
[39] G. Dennler, R. Chmielowski, S. Jacob, F. Capet, P. Roussel, S. Zastrow, K. Nielsch, I. Opahle, G.K.H. Madsen, Adv. Energy Mater. (2014) 1301581.
[40] A.H. Reshak, S. Auluck, Phys. B 358 (2005) 158.
[41] A.H. Reshak, Phys. B 369 (2005) 243–253.
[42] L. Joo-Hyoung, J. Wu, Phys. Rev. Lett. 104 (2010) 016602.
[43] F. Wu, H.Z. Song, J.F. Jia, X. Hu, Prog. Nat. Sci. Mater. Int. 23 (2013) 408–412.